

Space-time error control using a partition-of-unity dual-weighted residual method applied to low mach number combustion

Jan P. Thiele¹ and Thomas Wick^{1,2}

¹Leibniz University Hannover, Institut of Applied Mathematics, Welfengarten 1, 30167
Hannover, Germany

²Université Paris-Saclay, ENS Paris-Saclay, LMT – Laboratoire de Mécanique et Technologie,
91190 Gif-sur-Yvette, France

December 24, 2021

Abstract

In this work, a space-time scheme for goal-oriented a posteriori error estimation is proposed. The error estimator is evaluated using a partition-of-unity dual-weighted residual method. As application, a low mach number combustion equation is considered. In some numerical tests, different interpolation variants are investigated, while observing convergence orders and effectivity indices between true errors (obtained on a sufficiently refined mesh) and the error estimator.

Keywords:

low mach number combustion; dual weighted residuals; finite elements; adaptivity

AMS:

35K58, 49M29, 65N30, 65N50, 90A25

1 Introduction

This work is devoted to space-time goal-oriented a posteriori error control. Such space-time schemes for error estimation and adaptivity in time, space, or both, are of current interest with various applications in parabolic problems [14], incompressible Navier-Stokes equations [3, 4], dynamic Signorini, obstacle, and hyperbolic problems [6, 5, 12] and fluid-structure interaction [9, 10].

Our method is based on prior work, in which the dual-weighted error estimator is realized within a weak formulation using a partition-of-unity [13]. We note that another weak realization is achieved with the so-called filtering approach [7], which was already applied in [14, 3, 4] to space-time error control and adaptivity.

However, the extension of the partition-of-unity (PU) localization to space-time settings has not yet been established in the published literature. We provide a detailed algorithmic derivation of the error estimator and discuss the important ingredients. As numerical example, we consider a nonlinear low mach number combustion problem. A key part is the backward-in-time running adjoint problem.

One difficulty is that, due to Galerkin orthogonality, the adjoint problem must contain higher order information (see [2]) in the primal error part and vice versa in the adjoint error part. Recently, for stationary settings a new class of algorithms could be established by using interpolation information in a smart way [8]. For our proposed space-time setting we investigate the performance by simply choosing different combinations for the spatial finite elements, such as low-order $cG(1)/cG(1)$ and high-order equal elements $cG(2)/cG(2)$ as well as the natural approach $cG(1)/cG(2)$ (low order primal and higher order adjoint for the primal error part). These choices are investigated with respect to their convergence properties and evaluation of the effectivity indices. We will, however, limit ourselves to the variation of finite element orders in space and use the equal order approach for the temporal discretization. We also notice that some preliminary results on space-time adaptivity with the PU-DWR method are published in [15].

The outline of this work is as follows: In Section 2, the low mach number combustion equations are introduced and their weak formulation is provided. Next, in Section 3, the discretization with finite elements is described. In the main Section 4 a space-time PU-DWR error estimator is derived in detail. Finally, in Section 5 some numerical experiments are reported, that show the performance of our developments. The code for these simulations is based on our extension of the package `dwr-diffusion` [11] to solve nonlinear problems. The package itself uses `deal.II` [1] as the finite element library. We conclude our work in Section 6.

2 The Low Mach Number Combustion Equations

The nonlinear parabolic problem we want to investigate describes a combustion reaction under the low Mach number hypothesis. Under that hypothesis the dimensionless temperature θ and the concentration of the combustible species Y are not influencing the fluid velocity field.

For the special but important case of $v = 0$ all convection terms vanish and θ and Y are only influenced by diffusion and by the reaction mechanism in which Y combusts and raises the temperature. For constant diffusion coefficients we arrive at the following set of equations

$$\partial_t \theta - \Delta \theta = \omega(\theta, Y) \quad \text{in } \Omega \times (0, T), \quad (1)$$

$$\partial_t Y - \frac{1}{Le} \Delta Y = -\omega(\theta, Y) \quad \text{in } \Omega \times (0, T), \quad (2)$$

where the reaction is described by Arrhenius law

$$\omega(\theta, Y) = \frac{\beta^2}{2Le} Y e^{\frac{\beta(\theta-1)}{1+\alpha(\theta-1)}}. \quad (3)$$

The parameters are the Lewis number $Le = 1$, the gas expansion $\alpha = 0.8$ and the nondimensional activation energy $\beta = 10$.

Part of the boundary $\Gamma_R \subset \Gamma := \partial\Omega$ will be cooled. This can be described by a Robin condition $\partial_n \theta = -k\theta$. Following the standard procedure, we obtain the following space-time variational

formulation of our problem. Find $u = (\theta, Y)$ such that

$$\begin{aligned} A(u, \phi) &= (\partial_t \theta, \phi^\theta) + (\nabla \theta, \nabla \phi^\theta) + (\partial_t Y, \phi^Y) + (\nabla Y, \nabla \phi^Y) \\ &+ (\omega(\theta, Y), \phi^Y - \phi^\theta) + \int_0^T \int_{\Gamma_R} k \theta \phi^\theta ds dt = 0 =: F(\phi) \quad \forall \phi = (\phi^\theta, \phi^Y) \end{aligned} \quad (4)$$

where (f, g) describes the space-time scalar product defined as

$$(f, g) := \int_0^T \int_{\Omega} f g dx dt.$$

As the homogeneous Neumann condition on Γ_N is a natural condition it does not appear in the variational formulation. The inhomogeneous Dirichlet conditions on Γ_D are imposed as usual and inserted into the finite element spaces.

3 Discretization

As we want to use different finite elements for the temporal and the spatial test- and trial functions we will start by partitioning $[0, T]$ into M subintervals $I_n = (t_{n-1}, t_n]$, with the discretization parameter $k = t_n - t_{n-1}$. In time we will use piecewise constant discontinuous elements $\phi_k(t) \in dG(0)$. To be able to use different refined meshes over time, so called dynamic meshes, we will discretize Ω on each subinterval by a triangulation \mathcal{T}_h^n . Using quadrilaterals (in two-dimensional configurations) for the spatial triangulation, we can use continuous finite element functions $\phi_h(x) \in cG(p)$ of order p as test functions and trial functions. The fully discrete equations on each subinterval are then obtained by using $\phi_k h \in dG(0)cG(p)$ as test functions and trial functions in (4). For a more detailed look at the discretization and the corresponding finite element spaces see [14].

4 Space-Time PU-DWR Error Estimation

Denoting our quantity of interest by the goal functional $J(u)$, we obtain the Lagrange functional for minimizing the error in said quantity as

$$\mathcal{L}(u, z) = J(u) + F(z) - A(u, z). \quad (5)$$

As a first order optimality condition we obtain the KKT (Karush-Kuhn-Tucker) system and with it an auxiliary adjoint problem. In summary, we then have

$$\mathcal{L}'_u(u)(\psi, z) = J'_u(u)(\psi) - A'_u(u)(\psi, z) \stackrel{!}{=} 0 \quad (\text{adjoint problem}) \quad (6)$$

$$\mathcal{L}'_z(z)(u, \phi) = F(\phi) - A(u, \phi) \stackrel{!}{=} 0 \quad (\text{primal problem}) \quad (7)$$

Note that for nonlinear problems $A(u, z)$ is a semilinearform that is linear in z and that $F(z)$ is always a linear form. Thus, the directional derivative in direction ϕ w.r.t. to z , i.e. $A'_z(z)(u, \phi)$ coincides with $A(u, \phi)$. The same holds for linear goal functionals and linear problems resulting in the dual

problem $A(\psi, z) = J(\psi)$. Also note that the adjoint problem obtained by this derivation applies the temporal derivative to the test function. To rectify this, a partial integration in time is applied to $(\partial_t \psi, z)$, yielding $(\psi, -\partial_t z)$. This results in a problem that runs backwards in time and has a final condition instead of an initial condition.

4.1 Error Estimation

Following Proposition (2.1) in [2] we obtain the error representation

$$J(u) - J(u_{kh}) = \frac{1}{2} \mathcal{L}'_z(z_{kh})(u_{kh}, z - z_{kh}) + \frac{1}{2} \mathcal{L}'_u(u_{kh})(u - u_{kh}, z_{kh}) + \mathcal{R}, \quad (8)$$

where \mathcal{R} is a higher order remainder term. In many cases it is sufficient to approximate the error by only computing the primal residual i.e.

$$\begin{aligned} J(u) - J(u_{kh}) &\approx \mathcal{L}'_z(z_{kh})(u_{kh}, z - z_{kh}) \\ &= F(z - z_{kh}) - A(u_{kh}, z - z_{kh}) =: \rho_{kh}(u_{kh}, z - z_{kh}), \end{aligned} \quad (9)$$

which is also called primal error estimator. Subsequently the second term in the error representation is called adjoint error estimator $\rho_{kh}^*(u_{kh})(u - u_{kh}, z_{kh})$. Introducing the semidiscrete solutions u_k and z_k which are still continuous in space the primal error estimator can be further split into a temporal estimator ρ_k and a spatial estimator ρ_h

$$\begin{aligned} J(u) - J(u_{kh}) &= [J(u) - J(u_k)] + [J(u_k) - J(u_{kh})] \\ &\approx \rho_k(u_k, z - z_k) + \rho_h(u_{kh}, z_k - z_{kh}). \end{aligned} \quad (10)$$

4.2 Practical Evaluation

As the exact solutions u and z are unknown, we have to further approximate them to calculate the error estimators. For the temporal primal estimator, we will construct a piecewise linear solution $i_k^{(1)} z$ on each grid point by linear interpolation between the piecewise constant solutions z_n and z_{n-1} in the interval I_n .

For the spatial estimator we will look at three different approaches. The simplest approach is calculating u_{kh} with $dG(0)cG(1)$ elements and z_{kh} with $dG(0)cG(2)$ elements. Then, we assume z_{kh} to be the approximation of the exact solution and interpolate it down into $cG(1)$ in space obtaining $i_h^{(2,1)} z_{kh}$. This interpolation should be included in most finite element packages.

For also calculating the dual estimator we also need an approximation for u , which can be obtained by approximating u_{kh} and z_{kh} with $dG(0)cG(2)$ elements. Using the same interpolation as before we can approximate the discrete solutions as $\tilde{u}_{kh} := i_h^{(2,1)} u_{kh}$ and $\tilde{z}_{kh} := i_h^{(2,1)} z_{kh}$, while the exact solutions are approximated by u_{kh} and z_{kh} .

As this approach can be quite memory intensive, both u_{kh} and z_{kh} can be solved using $dG(0)cG(1)$ elements. The approximation for z can then be obtained by combining neighbouring $cG(1)$ elements into one large $cG(2)$ patch with the operator $i_{2h}^{(2)}$. The operator and the requirements for the mesh are

described in [7]. Using those interpolations we obtain the following primal estimators for the different approaches

$$\eta_k^{cG(1)/cG(1)} = F(i_k^{(1)} z_{kh} - z_{kh}) - A(u_{kh}, i_k^{(1)} z_{kh} - z_{kh}), \quad (11)$$

$$\eta_h^{cG(1)/cG(1)} = F(i_{2h}^{(2)} z_{kh} - z_{kh}) - A(u_{kh}, i_{2h}^{(2)} z_{kh} - z_{kh}), \quad (12)$$

for $u_{kh} \in dG(0)cG(1)$ and $z_{kh} \in dG(0)cG(1)$,

$$\eta_k^{cG(1)/cG(2)} = F(i_k^{(1)} i_h^{(2,1)} z_{kh} - i_h^{(2,1)} z_{kh}) - A(u_{kh}, i_k^{(1)} i_h^{(2,1)} z_{kh} - i_h^{(2,1)} z_{kh}), \quad (13)$$

$$\eta_h^{cG(1)/cG(2)} = F(z_{kh} - i_h^{(2,1)} z_{kh}) - A(u_{kh}, z_{kh} - i_h^{(2,1)} z_{kh}), \quad (14)$$

for $u_{kh} \in dG(0)cG(1)$ and $z_{kh} \in dG(0)cG(2)$,

$$\eta_k^{cG(2)/cG(2)} = F(i_k^{(1)} \tilde{z}_{kh} - \tilde{z}_{kh}) - A(\tilde{u}_{kh}, i_k^{(1)} \tilde{z}_{kh} - \tilde{z}_{kh}), \quad (15)$$

$$\eta_h^{cG(2)/cG(2)} = F(z_{kh} - \tilde{z}_{kh}) - A(\tilde{u}_{kh}, z_{kh} - \tilde{z}_{kh}), \quad (16)$$

for $u_{kh} \in dG(0)cG(2)$ and $z_{kh} \in dG(0)cG(2)$.

The corresponding dual estimators are obtained by the same interpolation operators, but applied to the primal solution u_{kh} and inserted into the adjoint problem.

$$\eta_k^{*cG(1)/cG(1)} = J'_u(u_{kh})(i_k^{(1)} u_{kh} - u_{kh}) - A'_u(u_{kh})(i_k^{(1)} u_{kh} - u_{kh}, z_{kh}) \quad (17)$$

$$\eta_h^{*cG(1)/cG(1)} = J'_u(u_{kh})(i_{2h}^{(2)} u_{kh} - u_{kh}) - A'_u(u_{kh})(i_{2h}^{(2)} u_{kh} - u_{kh}, z_{kh}) \quad (18)$$

$$\eta_k^{*cG(1)/cG(2)} = J'_u(u_{kh})(i_k^{(1)} u_{kh} - u_{kh}) - A'_u(u_{kh})(i_k^{(1)} u_{kh} - u_{kh}, i_h^{(2,1)} z_{kh}) \quad (19)$$

$$\eta_h^{*cG(1)/cG(2)} = J'_u(u_{kh})(i_{2h}^{(2)} u_{kh} - u_{kh}) - A'_u(u_{kh})(i_{2h}^{(2)} u_{kh} - u_{kh}, i_h^{(2,1)} z_{kh}) \quad (20)$$

$$\eta_k^{*cG(2)/cG(2)} = J'_u(\tilde{u}_{kh})(i_k^{(1)} \tilde{u}_{kh} - \tilde{u}_{kh}) - A'_u(\tilde{u}_{kh})(i_k^{(1)} \tilde{u}_{kh} - \tilde{u}_{kh}, \tilde{z}_{kh}), \quad (21)$$

$$\eta_h^{*cG(2)/cG(2)} = J'_u(\tilde{u}_{kh})(u_{kh} - \tilde{u}_{kh}) - A'_u(\tilde{u}_{kh})(u_{kh} - \tilde{u}_{kh}, \tilde{z}_{kh}). \quad (22)$$

4.3 Variational PU Localization

For use in adaptive refinement we need to obtain indicators η_K^n or η_i^n for each cell K or DoF i on the time interval I_n , such that

$$\eta = \sum_{n=1}^M \sum_{K \in \mathcal{T}_h^n} \eta_K^n = \sum_{n=1}^M \sum_{i \in \mathcal{T}_h^n} \eta_i^n. \quad (23)$$

We propose a DoF-wise partition of unity (PU) χ_i^n , with

$$\sum_{n=1}^M \sum_{i \in \mathcal{T}_h^n} \chi_i^n \equiv 1, \quad (24)$$

the simplest choice is $\chi_i^n \in dG(0)cG(1)$. Effectively, this leads to a spatial PU per time step, that is identical to the approach of [13] for stationary problems. The estimators are obtained by multiplying

the directions in the derivatives of the Lagrangian with the PU, which leads to the localization of the original error representation (8):

$$2[J(u) - J(u_{kh})]_i^n := \mathcal{L}'_z(z_{kh})(u_{kh}, (z - z_{kh})\chi_i^n) + \mathcal{L}'_u(u_{kh})((u - u_{kh})\chi_i^n, z_{kh}), \quad (25)$$

$$J(u) - J(u_{kh}) = \mathcal{R} + \sum_{n=1}^M \sum_{i \in \mathcal{T}_h} [J(u) - J(u_{kh})]_i^n. \quad (26)$$

Finally, inserting the PU into the estimators described in the previous subsection yields the error indicators for each space-time DoF.

5 Numerical Example

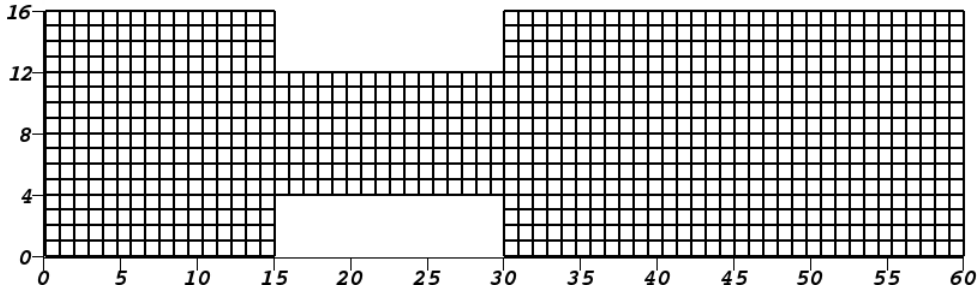


Figure 1: initial grid with $N = 896$ cells and $1970(cG(1)^2)$ and $7522(cG(2)^2)$ degrees of freedom.

In our numerical example, we solve the equations described in Section 2 on the geometry shown in Fig. 1. Here, the left edge of the domain Γ_D is kept at a constant temperature $\theta = 1$ without any combustible species $Y = 0$. The recessed area between $x = 15$ and $x = 30$ is the cooled Robin boundary Γ_R , with $\partial_n \theta = -0.1\theta$ and $\partial_n Y = 0$. On the rest of the boundary Γ_N homogeneous Neumann conditions are set.

The initial conditions are described by

$$\theta_0(x, z) = \begin{cases} 1, & x \leq 9, \\ e^{9-x}, & x > 9 \end{cases} \quad (27)$$

$$Y_0(x, z) = \begin{cases} 0, & x \leq 9, \\ 1 - e^{Le(9-x)}, & x > 9 \end{cases} \quad (28)$$

The functional of interest is the space-time averaged reaction rate

$$J(u) = \frac{1}{T|\Omega|} \int_0^T \int_{\Omega} \omega(\theta, Y) dx dt, \quad (29)$$

with final time $T = 60$.

The initial grid is solved with $k = 0.234375$, resulting in $M = 256$ time intervals.

5.1 Comparison of Error Estimators

To compare the estimators without influence of the adaptivity, the following simulations were done with global refinement in space and time. Tables 1 - 3 show the results for the error $J(u) - J(u_{kh})$ in comparison with the primal, adjoint and full estimators respectively. Since we use a different number of degrees of freedom for each approach, we decided to base the comparison on the number of time steps M and the number of spatial cells N . As a rough approximation the solution $(\theta, Y) \in cG(1)^2$ needs $2N$ and the solution $(\theta, Y) \in cG(2)^2$ needs $8N$ spatial degrees of freedom. As a $cG(1)$ representation of the solution is inserted as u_{kh} in (8), the error $J(u) - J(u_{kh})$ is evaluated in either the $cG(1)/cG(1)$ or the $cG(1)/cG(2)$ case. Note that the error would be larger for the projection of the $cG(2)$ solution into $cG(1)$ for the $cG(2)/cG(2)$ approach, as that interpolation simply uses the values at the vertex DoFs with the respective $cG(1)$ basis functions and discards all other parts of the solution.

Table 1: Primal estimators for different global refinement levels.

M	N	$J(u) - J(u_{kh})$	$\eta_{kh}^{cG(1)/cG(1)}$	$\eta_{kh}^{cG(1)/cG(2)}$	$\eta_{kh}^{cG(2)/cG(2)}$
256	896	$1.07197741e - 02$	$1.92058654e - 03$	$7.61264827e + 06$	$5.30861697e - 04$
512	3584	$2.48965242e - 03$	$6.43743177e - 04$	$4.08892798e - 01$	$2.34439679e - 04$
1024	14336	$5.67024544e - 04$	$2.61386699e - 04$	$1.32470408e - 03$	$2.02825765e - 04$
2048	57344	$1.11743216e - 04$	$1.08270274e - 04$	$1.62070260e - 04$	$1.02680294e - 04$

Table 2: Adjoint/dual estimators for different global refinement levels.

M	N	$J(u) - J(u_{kh})$	$\eta_{kh}^{cG(1)/cG(1)}$	$\eta_{kh}^{cG(1)/cG(2)}$	$\eta_{kh}^{cG(2)/cG(2)}$
256	896	$1.07197741e - 02$	$1.19648379e - 03$	$1.82646766e + 08$	$1.21421097e - 03$
512	3584	$2.48965242e - 03$	$8.33534627e - 04$	$2.79437497e + 00$	$7.95366447e - 04$
1024	14336	$5.67024544e - 04$	$4.25107914e - 04$	$4.21358177e - 03$	$4.21309997e - 04$
2048	57344	$1.11743216e - 04$	$2.74717107e - 04$	$3.83350535e - 04$	$1.70568548e - 04$

Table 3: Full estimators for different global refinement levels.

M	N	$J(u) - J(u_{kh})$	$\eta_{kh}^{cG(1)/cG(1)}$	$\eta_{kh}^{cG(1)/cG(2)}$	$\eta_{kh}^{cG(2)/cG(2)}$
256	896	$1.07197741e - 02$	$1.37575686e - 03$	$9.20610356e + 07$	$8.20354657e - 04$
512	3584	$2.48965242e - 03$	$5.59566023e - 04$	$1.60163388e + 00$	$5.14903063e - 04$
1024	14336	$5.67024544e - 04$	$3.32992866e - 04$	$2.54117001e - 03$	$2.74961514e - 04$
2048	57344	$1.11743216e - 04$	$1.77760869e - 04$	$2.55543805e - 04$	$1.25485484e - 04$

Comparing the results over all tables, we see that the equal order approaches perform relatively similar and better than the mixed order approach. Especially on lower refinement levels the $cG(1)/cG(2)$ results are orders of magnitude above the actual error. On closer inspection the adjoint solutions get larger with each time step, which leads to the estimator being dominated by the indicators on the

first few time intervals. As the codes for solving the $cG(2)$ adjoint problems for $cG(2)/cG(2)$ and $cG(1)/cG(2)$ basically only differ in the u_{kh} that is inserted in the assembly of the right hand side and the nonlinear part of the matrix, we surmise that the errors from inserting a lower order solution get amplified with each time step. This would also explain why this approach does not fail for stationary problems even on coarse meshes. In previous simulations we also saw that pairing the $cG(1)/cG(2)$ approach with solving the adjoint with $cG(1)$ elements in time led to worse results than the temporal equal order approach, even for the linear heat equation with the L_2 error as functional of interest. For adaptivity on dynamic meshes this is of course a considerable problem, as it is advisable to start with a coarse mesh to only capture the local behaviour of the solution/functional at each time interval.

When comparing the tables with each other, we see that for this problem the primal error estimator on itself performs better than the adjoint error estimator and is comparable to the full estimator. Overall, the $cG(1)/cG(1)$ approach is preferable as it is considerably cheaper to calculate compared to the $cG(2)/cG(2)$ approach for which multiple linear systems need to be solved with $\approx 8N$ unknowns (one solve for the adjoint and several solves for the primal Newton solver steps) instead of $\approx 2N$ unknowns. Additionally, the primal solution vectors have to be kept either in RAM or on hard disk as the adjoint is solved backwards in time, so the $cG(2)/cG(2)$ leads to a considerable increase in memory or storage demand. From a computational standpoint one can see why the $cG(1)/cG(2)$ approach would be a nice tradeoff between accuracy and memory demand as only a single linear solve per time step has to be performed on the larger set of unknowns.

5.2 Adaptive Results

When comparing the different estimators in the $cG(1)/cG(1)$ approach the primal estimator is closest to the actual error, so we decided to use this estimator as a basis for an adaptive simulation. As we have DoF-based indicators we compute cell-wise indicators to use build-in refinement strategies in `deal.II`. These are obtained by simply adding the four spatial indicators of the cell vertices. As a refinement strategy we chose fixed fraction marking in which the indicators are sorted and the $x\%$ of cells with the largest indicators are marked for refinement. The same strategy is applied to the time intervals for which the indicators are calculated as the sum over all temporal DoF-indicators on the corresponding spatial triangulation. As fractions we chose 50% for the temporal and 33% for the spatial refinement which leads to roughly $1.5M$ time intervals and $2N$ spatial cells per time interval compared to $2M$ and $4N$ for global refinement. Figure 2 shows that the exact error converges faster for adaptive refinement, when comparing the number of primal DoFs.

To see if our novel localization approach works well in capturing the local behaviour of the goal functional, Figures 3 and 4 show the evolution of the reaction rate ω over $[0, T]$ and the corresponding meshes. In all timesteps the combustion reaction is captured well by the fine cells. Additionally, for time steps after the flame passed the cooled rods, there is also some refinement around the sharp corners, which is to be expected.

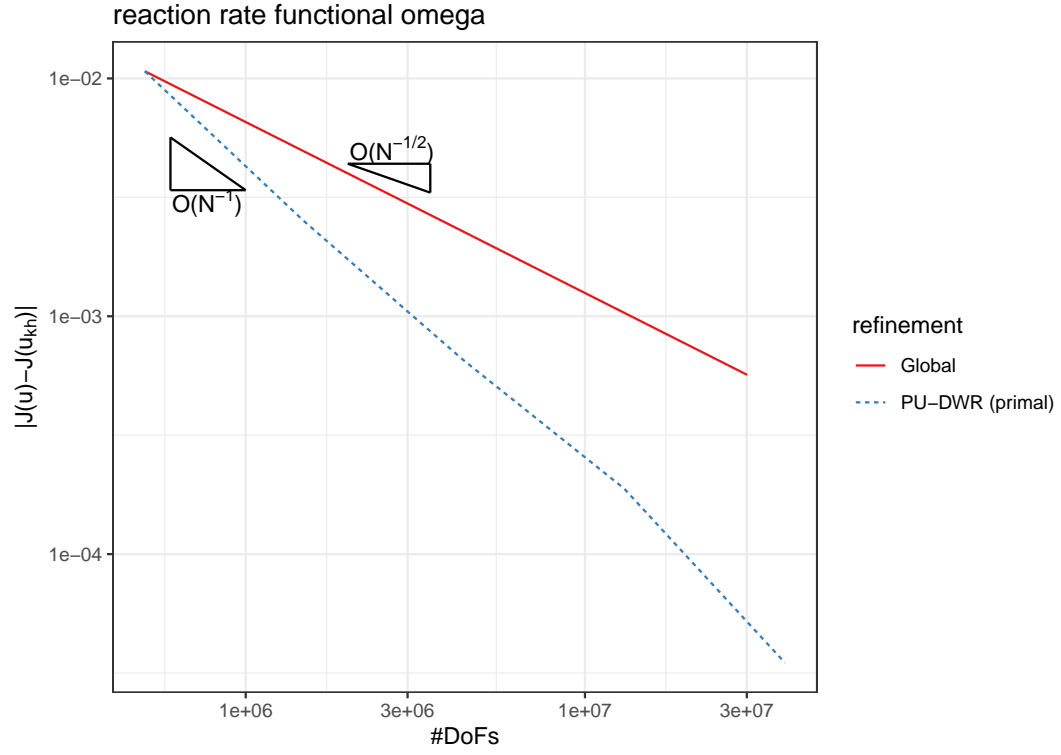


Figure 2: Comparison of the actual errors for global refinement vs. adaptive refinement with the primal $cG(1)/cG(1)$ estimator with marking 50% of the time intervals and 33% of the spatial cells on each interval for refinement.

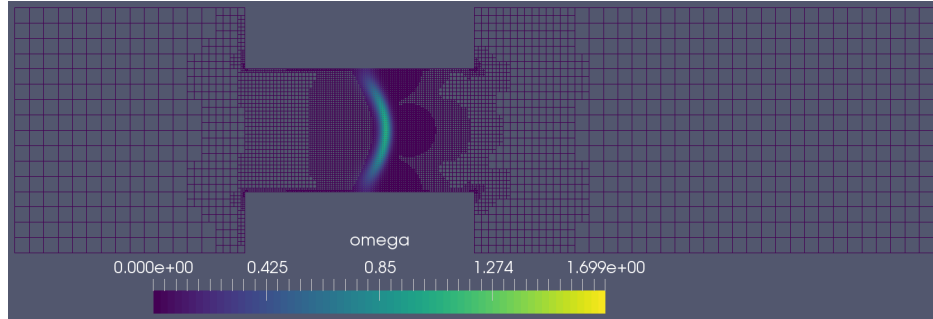


Figure 3: reaction rate ω at $t = 20$

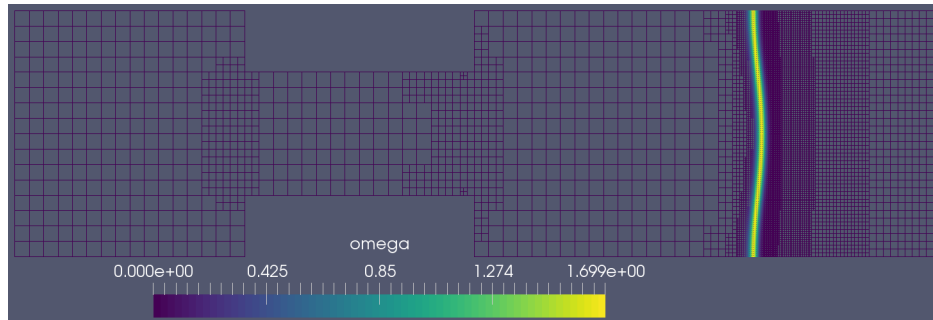


Figure 4: reaction rate ω at $t = 60$

6 Conclusions

In this work, we developed a space-time goal-oriented a posteriori error estimator using a newly developed partition-of-unity dual-weighted residual localization. As model problem we considered a nonlinear low Mach number combustion problem. Specific emphasis was on different space-time finite element combinations for the primal and adjoint subproblems. Therein, we detected a better performance for equal-order combinations of $cG(1)/cG(1)$ and $cG(2)/cG(2)$ type in comparison to a $cG(1)/cG(2)$ finite element. The reason has not yet been fully understood by us and needs further future investigations whether algorithmic or mathematical problems are the reason. Finally, some illustrations of locally adaptive meshes show that the error indicators obtained by our proposed method yield excellent findings in terms of resolving the local flame front.

References

- [1] D. Arndt, W. Bangerth, B. Blais, T. C. Clevenger, M. Fehling, A. V. Grayver, T. Heister, L. Heltai, M. Kronbichler, M. Maier, P. Munch, J.-P. Pelteret, R. Rastak, I. Tomas, B. Turcksin, Z. Wang, and D. Wells. The deal.II library, Version 9.2. *Journal of Numerical Mathematics*, 28(3):131–146, Sept. 2020.
- [2] R. Becker and R. Rannacher. An optimal control approach to a posteriori error estimation in finite element methods. *Acta Numerica, Cambridge University Press*, pages 1–102, 2001.
- [3] M. Besier. *Adaptive Finite Element methods for computing nonstationary incompressible Flows*. PhD thesis, University of Heidelberg, 2009.
- [4] M. Besier and R. Rannacher. Goal-oriented space-time adaptivity in the finite element galerkin method for the computation of nonstationary incompressible flow. *Int. J. Num. Meth. Fluids*, 70:1139–1166, 2012.
- [5] H. Blum, A. Rademacher, and A. Schröder. Space adaptive finite element methods for dynamic obstacle problems. *Electronic Transactions on Numerical Analysis*, 32:162–172, 2008.
- [6] H. Blum, A. Rademacher, and A. Schröder. Space adaptive finite element methods for dynamic signorini problems. *Computational Mechanics*, 44(4):481–491, 2009.
- [7] M. Braack and A. Ern. A posteriori control of modeling errors and discretization errors. *Multiscale Model. Simul.*, 1(2):221–238, 2003.
- [8] B. Endtmayer, U. Langer, and T. Wick. Reliability and efficiency of dwr-type a posteriori error estimates with smart sensitivity weight recovering. *Computational Methods in Applied Mathematics*, 21(2), 2021.
- [9] L. Failer. *Optimal Control of Time-Dependent Nonlinear Fluid-Structure Interaction*. PhD thesis, Technical University Munich, 2017.

- [10] L. Failer and T. Wick. Adaptive time-step control for nonlinear fluid-structure interaction. *Journal of Computational Physics*, 366:448 – 477, 2018.
- [11] U. Köcher, M. P. Bruchhäuser, and M. Bause. Efficient and scalable data structures and algorithms for goal-oriented adaptivity of space–time FEM codes. *SoftwareX*, 10:100239, July 2019.
- [12] A. Rademacher. *Adaptive finite element methods for nonlinear hyperbolic problems of second order*. PhD thesis, Technische Universität Dortmund, 2009.
- [13] T. Richter and T. Wick. Variational localizations of the dual weighted residual estimator. *Journal of Computational and Applied Mathematics*, 279(0):192 – 208, 2015.
- [14] M. Schmich and B. Vexler. Adaptivity with dynamic meshes for space-time finite element discretizations of parabolic equations. *SIAM J. Sci. Comput.*, 30(1):369 – 393, 2008.
- [15] J. Thiele and T. Wick. Space-time pu-dwr error control and adaptivity for the heat equation. *Proceedings in Applied Mathematics and Mechanics*, accepted, 2021.